NATIONAL INITIATIVE ON UNDERGRADUATE SCIENCE (NIUS) - ASTRONOMY
2017

MORPHOLOGICAL DISTRIBUTION OF MOLECULAR CLOUDS IN IRAS 16164-5046

December 20, 2017

Aditya Sharma
Divij Mishra
Jaidev Ashok
Sandesh S. Kalantre

Contents

Chapter 1

Introduction

1.1 Molecular Clouds

Molecular clouds play an important role in star formation, being the precursors to all stars. These are huge entities which may extend to several parsecs in size, and can be as massive as 10^4 Solar Masses or more [Blitz, 1993]. The conditions observed in the core of molecular clouds are believed to be optimum for star formation, earning them the *moniker of star nursery*. However, we know little about the morphological distribution.

In this project, we use emission in far infrared from cold dust to study the morphological distribution and physical properties associated with clumps in molecular clouds.

1.2 Related Work

We observe the molecular cloud, IRAS 16164-5046 (Gal. Coordinates: l = 332.8, b = -0.56), which lies in the galactic plane. The distance to the cloud, 3.6 kpc, is adopted from [Karnik et al., 2001]. Emission maps of ^{13}CO and C1 have indicated a velocity of $-57\,\mathrm{km\,s^{-1}}$ (Lo, 2014), while kinematic analysis of H109 recombination line indicates a velocity of $-57.2\,\mathrm{km\,s^{-1}}$ [Lockman et al., 1979] Molecular column densities have been calculated using empirical relations from CO and have been estimated to be around $10^{22}\,\mathrm{cm^{-2}}$ (Lo, 2014).

1.3 Dataset

In our report, we have analyzed our source in far-infrared with images from Herschel Space Observatory and ATLASGAL survey. Images at 70 µm and 160 µm were captured using PACS

	70 µm	250 µm	350 µm	500 µm	870 µm
Pixel Size	2"	6"	10"	14"	6"
Angular Resolution	5"	18.1"	24.9"	36.4"	18"

(Photodetector Array Camera and Spectrometer) while those at 250 µm, 350 µm and 500 µm were captured using SPIRE (Spectral and Photometric Imaging Receiver). The 160 µm image was not included in our analysis due to the presence of artifacts. The pixel sizes and angular resolutions of all the raw images are listed in Table 1.

The 870 µm image was taken from the ATLASGAL Survey. The flux uncertainties were assumed to be 15% for Herschel images as well as ATLASGAL images. See Appendix for details on image processing. The final four cropped images are presented below.

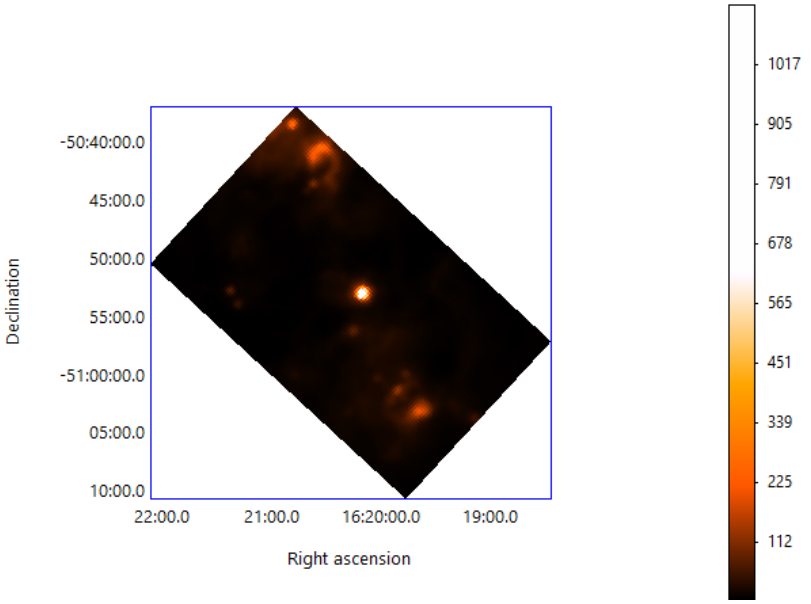

Figure 1.1: 70µm HERSCHEL

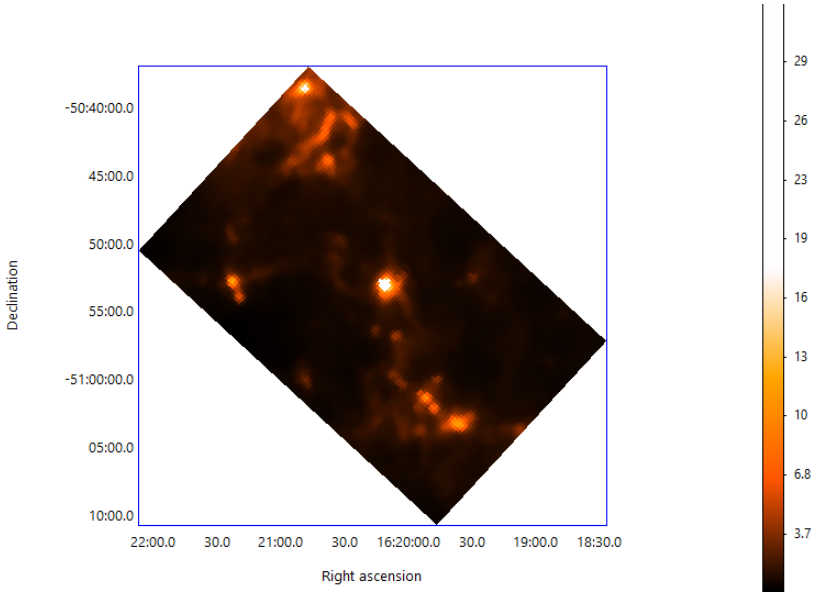

Figure 1.2: 350μm HERSCHEL

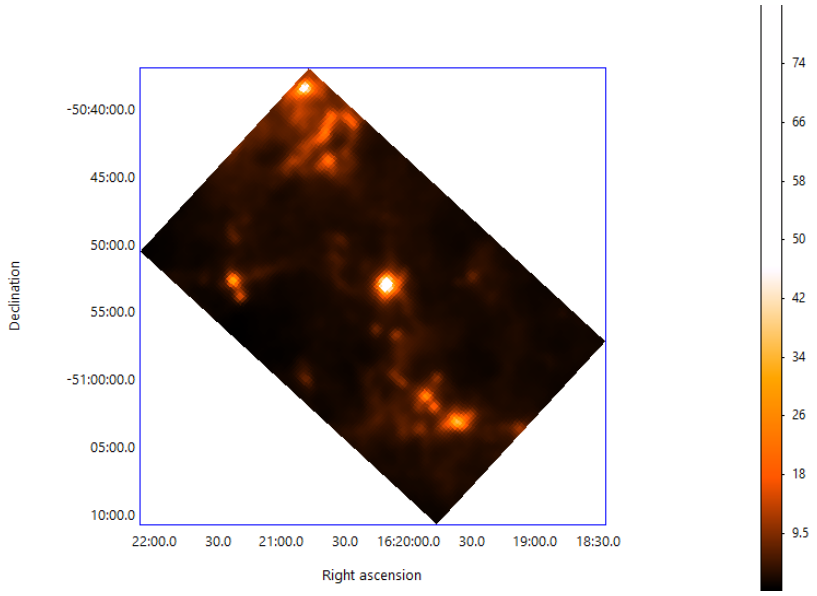

Figure 1.3: 500μm HERSCHEL

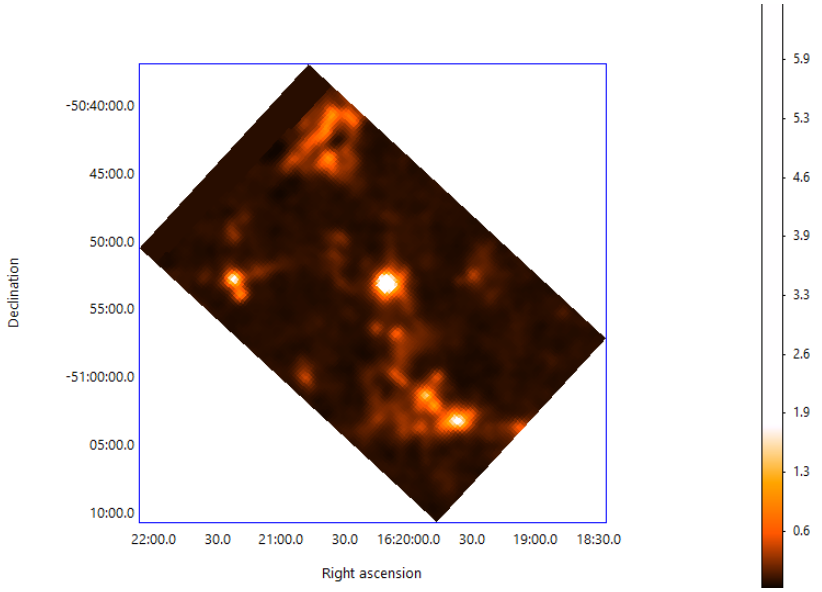

Figure 1.4: 870µm ATLASGAL

Chapter 2

Column Density and Temperature Calculations

The spectral energy distribution (SED) of a blackbody is a function of the temperature. Moreover, the observed intensity is affected by the column density present along the line of sight of the observer. In order to study the dust temperature and the column density, we used the infrared emission obtained in HERSHEL (70, 350 and 500 µm and ATLASGAL (870 µm). The emission in these four wavelength bands was used to fit a modified -blackbody spectrum.

2.1 SED FORMULATION

We adopted a modified black-body spectrum from ([Battersby et al., 2011]).

$$F_\nu = \Omega B_\nu(T_d)(1 - e^{-\tau_\nu})$$

where Ω is the solid angle, B_ν is the Planck spectrum as a function of temperature T_d and τ_ν is the optical depth at frequency ν. We used,

$$\tau_\nu = \mu m_H \kappa_\nu N$$

where $\mu = 2.8$ is the mean molecular mass, m_H is the mass of hydrogen, κ_ν is the opacity as a function of ν and N is the column density.

We used a power-law model for the opacity ([Ward-Thompson et al., 2010].

$$\kappa_\nu = 0.1\left(\frac{\nu}{1000\,\mathrm{GHz}}\right)^\beta \mathrm{cm}^2\mathrm{g}^{-1}$$

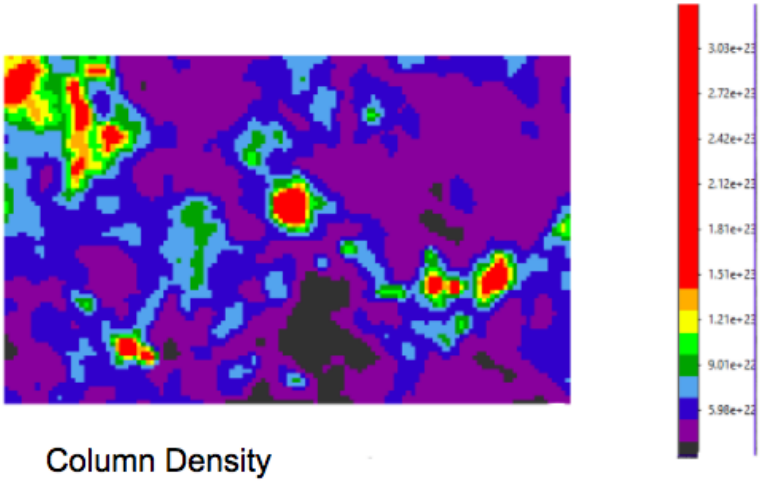

Figure 2.1: Column density calculated from the SED fitting

2.2 FITTING RESULTS

We did the SED fitting at each pixel in the convoluted images and obtained column density and temperature maps. The spectral index was fixed to $\beta = 3$ since we had only four points in the spectrum and leaving it as a free parameter did not always lead to good fits. The fitting was done using the `scipy.optimize.curve_fit` routine from the Python package SciPy which uses the nonlinear least-squares Marquardt-Levenberg algorithm. Figure shows column density and temperature maps from the fitting.

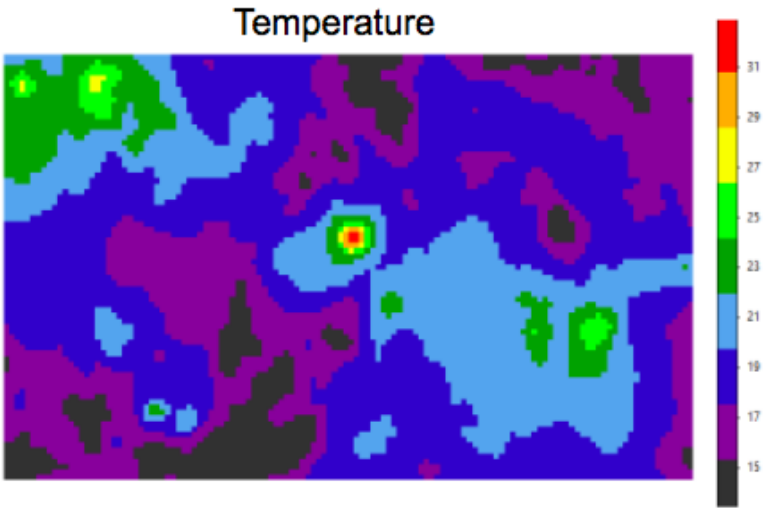

Figure 2.2: Temperature calculated from the SED fitting

Chapter 3

Finding Clumps

3.1 Algorithms

We use the 870 µm ATLASGAL images for the purpose of clump finding. The algorithms employed are the FellWalker algorithm [Berry, 2014] and the 2D-ClumpFind algorithm, the two-dimensional counterpart of the original ClumpFind algorithm [Williams et al., 1994]

The FellWalker algorithm works by tracing 'walks' to a peak from every pixel in the data image, seeking the step of steepest ascent from the center of every 3x3 pixel grid. The walk ends when a peak or a local maximum is reached, with a check on an extended neighbourhood to avoid pathways ending in bad (high noise) pixels.

The 2D-ClumpFind algorithm begins at a peak and contours the data at set or automatically calculated intervals to identify clumps.

In our analysis, clump-finding occurs over a spatial column density distribution for dust emissivity index β= 3 obtained from the modified blackbody curve fitting in section 2.2. Following this, the clumps were manually traced with polygons with some allowance in the region outside the clumps. We base our calculations and plots on these traced clumps in the following sections.

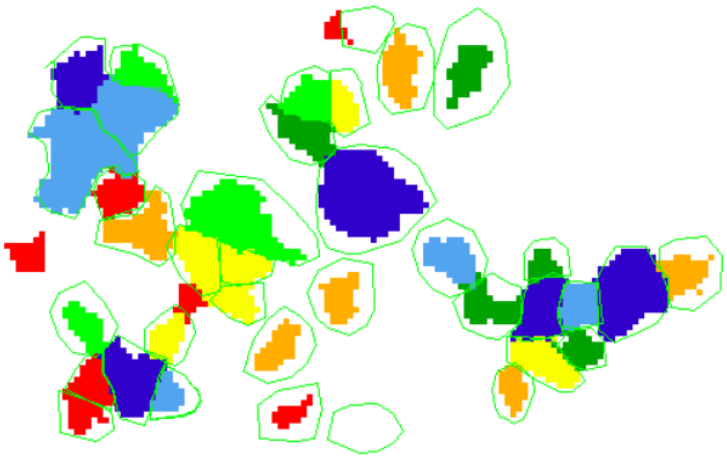

Figure 3.1: Clumps produced from the ClumpFind routine

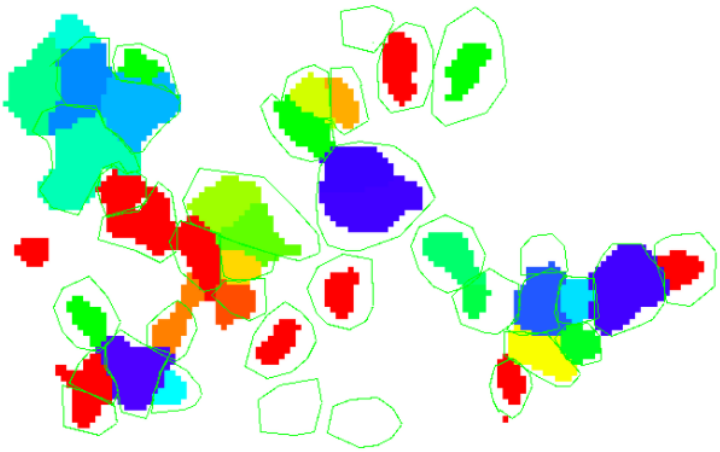

Figure 3.2: Clumps produced from the FelWalker routine

3.2 Our results

3.3 Clump SED and parameters

Parameter	Value
Contour height	1.0×10^{21}
Beam FWHM	2.0
Minimum Pixels	9
RMS Noise	2.67×10^{22}
Threshold value	5.0×10^{22}

Table 3.1: Parameters used for ClumpFind

Parameter	Value
Flat slope	0.0
Beam FWHM	2.0
Minimum dip	2.0×10^{22}
Minimum Peak Height	5.0×10^{22}
Minimum Pixels	9
RMS Noise	0.0
Threshold value	5.0×10^{22}

Table 3.2: Parameters used for FellWalker

A clump is determined if it is larger than 9 pixels (approximately the beam size). We use a threshold of $5.0 \times 10^{22}\,\mathrm{g\,cm^{-2}}$ for both the algorithms, and a contour height of $1.0 \times 10^{21}\,\mathrm{g\,cm^{-2}}$ for the ClumpFind algorithm. Peak column density over the entire region was $3.33 \times 10^{23}\,\mathrm{g\,cm^{-2}}$. In both cases, we set the AllowEdge parameter to 0 [FALSE] to reject clumps that exist only partially within the field of view.

With similar threshold levels, FellWalker produced a total of 20 clumps, and 2D-ClumpFind produced 41 clumps in all. We notice that ClumpFind tended to split clumps into finer sections for a similar set of parameters. We choose to borrow results from both the algorithms for greater consistency with observations of the eye, outlining 36 usable clumps and determining their respective intrinsic properties.

3.4 CLUMP EVOLUTION STAGE RESULTS

To find the relative evolutionary stages of the clumps, we categorize our clumps based on the criteria put forth by [Chambers et al., 2009] for Infrared Dark Clouds (IRDCs), which was further improved upon by [Battersby et al., 2010] by considering radio peaks in the classification. The initial stage of any region of the molecular cloud is the Quiescent stage (Q) which later evolves into the Active stage (A). Since Quiescent clumps are dormant regions, star formation is yet to begin in them. Hence, they don't show traces of MIR emission, i.e. 8 µm and 22 µm. Conversely, any traces of either 8 µm or radio peaks indicate an ongoing star formation process and hence these clumps are classified as Active/Evolved Clumps. The presence of 22 µm peaks alone, with MIR peaks absent, suggests an Intermediate Stage of evolution for the clump. Table 5 presents the above categorisation for the clumps we analyzed.

Clump number	Mass (10^3 solar units)	8 µm peaks	22 µm peaks	Radio peaks	Evolutionary category	Luminosity (10^5 solar units)
1	4.97	No Data	No Data	N	-	13.57
3	19.33	No Data	No Data	N	-	6.68
4	4.03	No Data	No Data	N	-	2.12
5	7.61	No Data	No Data	N	-	1.87
6	6.80	No Data	No Data	N	-	4.22
7	3.33	N	No Data	N	-	1.32
8	3.95	N	No Data	N	-	1.53
9	11.30	N	No Data	N	-	6.21
10	4.48	N	No Data	N	-	3.69
16	5.09	N	No Data	N	-	0.83
17	4.43	N	No Data	N	-	4.54
21	4.87	N	No Data	N	-	2.37
23	4.13	N	No Data	N	-	1.00
26	8.56	N	Y	N	-	7.97
27	7.06	N	No Data	N	-	7.72
28	3.81	N	No Data	N	-	7.21
29	5.93	N	No Data	N	-	8.06
30	8.36	Y	No Data	N	-	15.12
32	5.35	N	No Data	N	-	14.40
35	7.02	N	No Data	N	-	4.50
36	4.83	N	No Data	N	-	6.36
2	26.84	No Data	No Data	Y	A	16.25
12	16.64	Y	N	N	A	3.69
19	30.46	Y	Y	Y	A	19.66
31	3.29	Y	Y	N	A	10.30
33	3.49	N	No Data	Y	A	10.36
34	19.06	Y	No Data	Y	A	19.31
11	5.89	N	N	N	Q	1.73
13	3.64	N	N	N	Q	1.53
14	3.92	N	N	N	Q	1.08
15	6.78	N	N	N	Q	1.12
18	6.94	N	N	N	Q	1.84
20	6.75	N	N	N	Q	2.81
22	4.54	N	N	N	Q	1.88
24	8.17	N	N	N	Q	1.46
25	12.43	N	N	N	Q	3.53

Chapter 4

Discussion

4.1 YSOs

Young Stellar Object is a star in its early stages of formation/evolution. They are the collapsing cores of huge molecular clouds which become future stars. These Young Stellar Objects have characteristic Spectral Energy Distribution which help to categorize them into various types based on the evolutionary stages. The YSO Formation regions in dense cores together with the Radiation continuum helps us to categorize clumps detected as Active/Intermediate/Quiescent.

4.2 OVERLAYS WITH OTHER RESULTS

The following Column Density and Temperature Plots have been overlayed with the Young Stellar Objects categorized on the basis of criteria proposed by (Allen et al 2004) and 2MASS (Lada 1987).

Color Of Marked YSO	Class
Green	Class 1
Red	Class 2
Blue	Intermediate

Table 4.1: Allen Criterion

Color Of Marked YSO	Class
Green	Class 1
Red	Class 2

Table 4.2: 2Mass Criterion

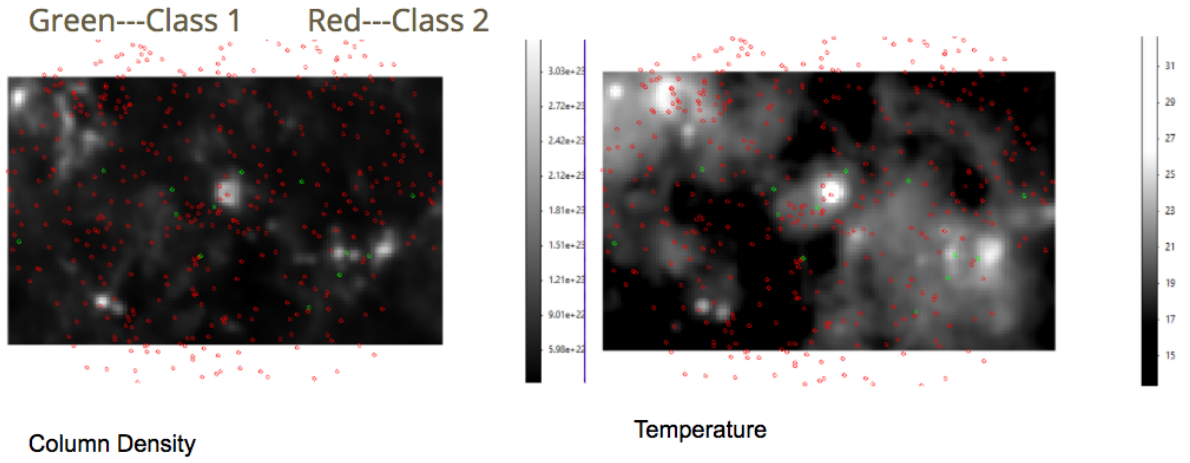

Figure 4.1: YSO overlay with 2MASS criterion

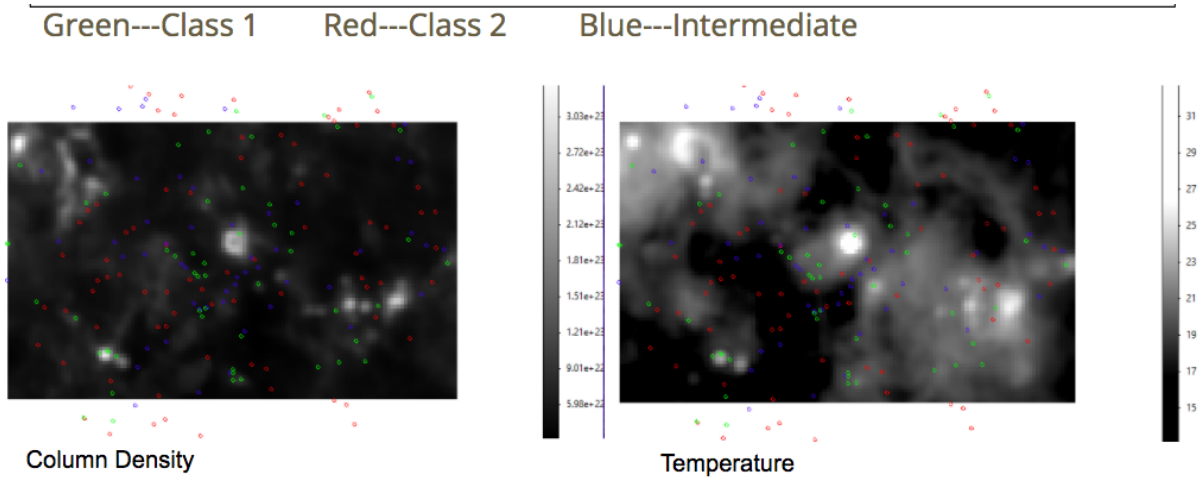

Figure 4.2: YSO overlay with Allen criterion

Chapter 5

Conclusions

- The column density was of the order $1 \times 10^{23}\,\mathrm{cm}^{-2}$.
- The temperature was 10 - 35 K.
- FellWalker produced 38 clumps, while ClumpFind produced 41 clumps.
- The clump masses were 5E3 to 3E4 Solar Masses, luminosities 1E5 to 1E6 Solar Luminosities.
- The clumps were classified in active and quiescent categories.
- We overlaid YSOs from the 2MASS and Allen criteria on our column density and temperature maps.
- The solid line in the log-log plot of Bolometric Luminosity and Mass of Clump separates the upper 'Envelope Clearing Phase' from the lower region of 'Accretion phase' for high mass protostellar objects like the clumps we observed (Molinari 2008)

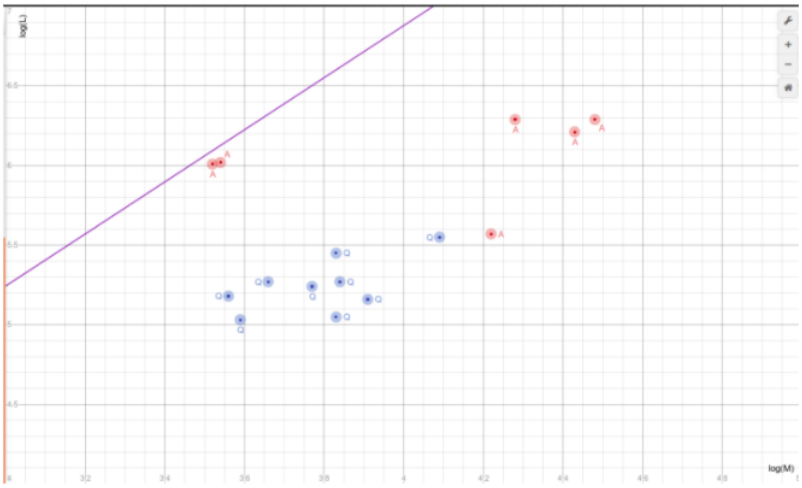

Figure 5.1: Mass-Luminosity for the clumps found laid on the plot from (Molinari 2008)

Appendix A

Initial Image Processing

We begin with PACS 70 μm, SPIRE 250 μm, 350 μm and 500 μm, and ATLASGAL 870 μm images of varied angular resolutions, pixel sizes, and data units. We determine the image of lowest resolution, which here, is the SPIRE 500 μm image with an angular resolution of 14 arcseconds. For plotting spectral index maps, each image is required to have the same resolution, pixel size, and data unit. We achieve this by employing the Herschel Interactive Processing Environment (HIPE) and Image Reduction and Analysis Facility (IRAF). We do so by first converting the units of the SPIRE images to Jy/pixel and convolving and regridding the 250 μm and 350 μm images taking the base image as 500 μm. Following this, we add units to header files of 70 μm and 870 μm images, convert these to Jy/pixel, and similarly convolve and regrid them with base image 500 μm. A rectangular crop is then made using pixel coordinates, now common to all images, around the region of interest, producing a sub-image of 128 x 79 pixels for each wavelength. As a final step, a crop is taken at an appreciable distance from the object centre devoid of diffuse emissions or bright objects in all wavelength bands as sky image for the background subtraction procedure.

Bibliography

[Battersby et al., 2011] Battersby, C., Bally, J., Ginsburg, A., Bernard, J. P., Brunt, C., Fuller, G. A., Martin, P., Molinari, S., Mottram, J., Peretto, N., Testi, L., and Thompson, M. A. (2011). Characterizing Precursors to Stellar Clusters with Herschel.

[Battersby et al., 2010] Battersby, C., Bally, J., Jackson, J. M., Ginsburg, A., Shirley, Y. L., Schlingman, W., and Glenn, J. (2010). An infrared through radio study of the properties and evolution of IRDC clumps. *Astrophysical Journal*, 721(1):222–250.

[Berry, 2014] Berry, D. (2014). FellWalker - a Clump Identification Algorithm.

[Blitz, 1993] Blitz (1993). Giant Molecular Clouds.

[Chambers et al., 2009] Chambers, E. T., Jackson, J. M., Rathborne, J. M., and Simon, R. (2009). Star formation activity of cores within infrared dark clouds. *Astrophysical Journal, Supplement Series*, 181(2):360–390.

[Karnik et al., 2001] Karnik, A. D., Ghosh, S. K., Rengarajan, T. N., and Verma, R. P. P. (2001). Study of star formation in RCW 106 using far-infrared observations. 302(December):293–302.

[Lockman et al., 1979] Lockman, F. J., Radio, N., Observatory, A., Bank, G., and Virginia, W. (1979). No Title. pages 761–781.

[Ward-Thompson et al., 2010] Ward-Thompson, D., Kirk, J. M., André, P., Saraceno, P., Didelon, P., Könyves, V., Schneider, N., Abergel, A., Baluteau, J. P., Bernard, J. P., Bontemps, S., Cambrésy, L., Cox, P., Di Francesco, J., Di Giorgio, A. M., Griffin, M., Hargrave, P., Huang, M., Li, J. Z., Martin, P., Men'shchikov, A., Minier, V., Molinari, S., Motte, F., Olofsson, G., Pezzuto, S., Russeil, D., Sauvage, M., Sibthorpe, B., Spinoglio, L., Testi, L., White, G., Wilson, C., Woodcraft, A., and Zavagno, A. (2010). A Herschel study of the properties of starless cores in the Polaris Flare dark cloud region using PACS and SPIRE. (14618):1–5.

[Williams et al., 1994] Williams, J. P., de Geus, E. J., and Blitz, L. (1994). Determining Structure in Molecular Clouds. *Apj*, 428:693.